Frontiers of Information Technology & Electronic Engineering
www.jzus.zju.edu.cn; engineering.cae.cn; www.springerlink.com
ISSN 2095-9184 (print); ISSN 2095-9230 (online)
E-mail: jzus@zju.edu.cn

# A novel algorithm to counter cross-eye jamming based on a multi-target model*

Zhi-yong SONG†‡, Xing-lin SHEN, Qiang FU

*National Key Laboratory of Science and Technology on ATR, National University of Defense Technology, Changsha 410073, China*

†E-mail: songzhiyong08@nudt.edu.cn

Received June 25, 2018; Revision accepted May 9, 2019; Crosschecked July 12, 2019

**Abstract:** Cross-eye jamming is an electronic attack technique that induces an angular error in the monopulse radar by artificially creating a false target and deceiving the radar into detecting and tracking it. Presently, there is no effective anti-jamming method to counteract cross-eye jamming. In our study, through detailed analysis of the jamming mechanism, a multi-target model for a cross-eye jamming scenario is established within a random finite set framework. A novel anti-jamming method based on multi-target tracking using probability hypothesis density filters is subsequently developed by combining the characteristic differences between target and jamming with the releasing process of jamming. The characteristic differences between target and jamming and the releasing process of jamming are used to optimize particle partitioning. Particle identity labels that represent the properties of target and jamming are introduced into the detection and tracking processes. The release of cross-eye jamming is detected by estimating the number of targets in the beam, and the distinction between true targets and false jamming is realized through correlation and transmission between labels and estimated states. Thus, accurate tracking of the true targets is achieved under severe jamming conditions. Simulation results showed that the proposed method achieves a minimum delay in detection of cross-eye jamming and an accurate estimation of the target state.

**Key words:** Particle identity labels; Probability hypothesis density; Cross-eye jamming; Anti-jamming; Random finite set; Monopulse radar

https://doi.org/10.1631/FITEE.1800394 **CLC number:** TN973.3

## 1 Introduction

Cross-eye jamming is an angular deception technique that attempts to deceive a tracking radar about the true position of its target by recreating the worst case angular error due to glint (du Plessis et al., 2011). This type of jamming is employed mainly for self-protection in aircrafts, ships, and other platforms, and it is considered to be one of the most promising electronic counter measures (ECMs). Compared with non-coherent jamming approaches, such as towed radar active decoys, cross-eye jamming is essentially a form of coherent jamming, does not require the jammer be located apart from the platform, and can produce a large angle deviation away from the target. As an advanced electronic attack (EA) strategy, cross-eye jamming technology is gradually maturing with the wide application to digital radio frequency memory (DRFM) technology. A cross-eye jamming verification test system was established by the Pretoria University, and darkroom and outfield tests were conducted to verify the effectiveness of the two-source retrodirective cross-eye jamming (du Plessis et al., 2011). The defensive aid sub-system (DASS) deployed by the Euro Typhoon Fighter verified the performance of cross-eye jamming on an aircraft platform for several times. The Sorbstiya and SAP-518 jamming pods on Russia's Su-27 and Su-30/32/33 fighters all have the ability to achieve cross-eye jamming (KRET, 2014).

‡ Corresponding author

* Project supported by the National Natural Science Foundation of China (No. 61401475)

ORCID: Zhi-yong SONG, http://orcid.org/0000-0002-3833-0510

Cross-eye jamming brings about a threat to the angle tracking used by monopulse radar; however, there have been few studies that considered counteracting the angular deception of cross-eye jamming. The polarization characteristic was introduced to detect the presence of coherent interference based on the polarization response difference between the target and jamming, although many polarization channels required by this method necessitated an upgrade of the radar system hardware (Li et al., 2013). The front-edge tracking method was proposed to recognize the presence of jamming using the range differences between target echoes and jamming signals (Xue et al., 2011), while the DRFM technology combined with the range gate pull-off (RGPO) method eliminated these differences. At the same time, multi-mode composite radar (Wu et al., 2011; Bai and Wang, 2013) and multi-base radar (Zhao et al., 2014; Li and Shen, 2015) showed great promise for anti-jamming, but they involved the use of multi-sensor fusion and are highly complex systems. These existing countermeasures for cross-eye jamming heavily depend on the radar system configuration and hardware conditions, thus limiting their popularization and application. These limitations are good reasons to explore an anti-jamming algorithm that can use an advanced signal and data processing algorithm based on the existing system resources without incurring additional hardware overhead.

In the implementation of cross-eye jamming, the jammer first captures the tracking gate in the monopulse radar and then generates jamming signals to deceive the radar point toward an artificial target, which is far away from the true target. The signal power of the jamming is much larger than that of the target. The powerful jamming signal suppresses and covers the true target echo, and makes it difficult to detect the target based on the echo of the sum channel (du Plessis, 2012, 2016). It is feasible to improve the target detection probability by decreasing the detection threshold, which will reduce the loss of target information. However, a lower threshold of detection will increase the false alarm probability, resulting in the failure of the traditional multi-target tracking methods that are based on data association. The low threshold of detection introduces enormous challenges in state estimation and identity recognition of the true target.

The recent and rapid development of finite set statistics (FISST) theory provides a new theoretical framework for joint detection and tracking of a target under complex conditions using a random finite set (RFS) (Mahler, 2007). This involves modeling the complex scenes and states using a Bayesian framework, taking into consideration elements, such as state space, observation space, false alarms, target missing, target appearance/disappearance, and varying tracking numbers (Mahler, 2014). The models developed under a Bayesian framework have great potential to realize accurate detection and stable tracking under cross-eye jamming. In particular, various approaches for tracking continuity with a Bayes filter, such as labeling (Lin et al., 2006; Clark and Bell, 2007; Xiao et al., 2015) and dyeing (Li et al., 2014), provide the possibility to realize target recognition in complex environments.

In this study, cross-eye jamming is analyzed and a monopulse radar measurement environment is developed using RFSs in a Bayesian framework. Based on a probability hypothesis density (PHD) filter for multi-target tracking, the difference in features between target and jamming is used to optimize particle partitions, and identity labels are used to represent the characteristics of targets, which are present within the radar beam. Through association and interaction of the estimated states and identity labels, the release of the cross-eye jamming is detected with high correct probability and small delay. On this basis, accurate state estimation of the target and correct target recognition are realized. The effectiveness of the algorithm is experimentally validated.

## 2 Signal and cross-eye jamming model

### 2.1 Model for target and jamming

The purpose of cross-eye jamming is to induce an angular error in the radar system, thus deceiving the monopulse radar into detecting an artificial target located away from the true target. The cross-eye jamming scenario is shown in Fig. 1 (du Plessis et al., 2009). Assume that the phase-comparison monopulse radar consists of two identical antennas separated by a distance $d_p$ (denoted by circles in Fig. 1). The cross-eye elements are linearly separated by $d_c$ at a range of $r$, with an angular separation of $2\theta_e$ as seen

from the radar (denoted by crosses in Fig. 1). The directions to the top and bottom cross-eye antennas are $\theta_r+\theta_c$ and $\theta_r-\theta_c$, respectively. $\theta_e$ can be determined as follows:

$$\theta_e=\frac{d_c/2\cos\theta_c}{r\pm d_c/2\sin\theta_c}\approx\frac{d_c}{2r}\cos\theta_c, \tag{1}$$

where $r$ is much greater than $d_c$.

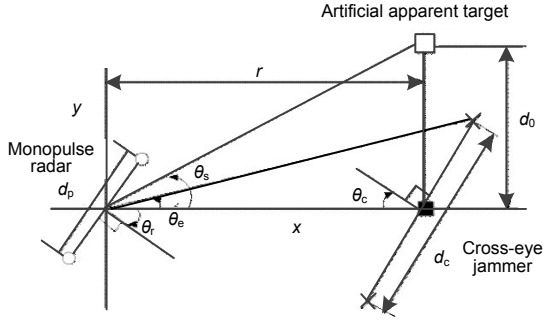


**Fig. 1 Geometric depiction of cross-eye jamming and its effect on detection by the monopulse radar**
$d_0$ denotes the distance between the apparent target and platform center

The normalized sum- and difference-channel gains in the direction $\theta_r$ measured from the boresight are given as follows:

$$\begin{cases}S_g=P_r(\theta_r)\cos\left(\beta\dfrac{d_r}{2}\sin\theta_r\right),\\ D_g=\mathrm{j}P_r(\theta_r)\sin\left(\beta\dfrac{d_r}{2}\sin\theta_r\right),\end{cases} \tag{2}$$

where $P_r(\theta_r)$ is the normalized gain of two antenna elements.

Similarly, the normalized sum- and difference-channel returns for the cross-eye jammer in isolation from the jammer antennas symmetrically positioned around $\theta_r=0$ are given as (du Plessis, 2012)

$$\begin{aligned}S_j=&P_r(\theta_r-\theta_e)P_c(\theta_c-\theta_e)P_r(\theta_r+\theta_e)P_c(\theta_c+\theta_e)\\&\cdot\frac{1}{2}(1+ae^{j\phi})\left[\cos(2k)+\cos(2k_c)\right],\end{aligned} \tag{3}$$

$$\begin{aligned}D_j=&P_r(\theta_r-\theta_e)P_c(\theta_c-\theta_e)P_r(\theta_r+\theta_e)\\&\cdot P_c(\theta_c+\theta_e)\cdot\mathrm{j}\frac{1}{2}\left[(1+ae^{j\phi})\sin(2k)\right.\\&\left.+(1-ae^{j\phi})\sin(2k_c)\right],\end{aligned} \tag{4}$$

where $P_c(\theta)$ is the normalized gain of the cross-eye jammer antenna elements with the angle measured from broadside.

$$\begin{cases}k=\beta\dfrac{d_r}{2}\sin\theta_r\cos\theta_e\approx\beta\dfrac{d_r}{2}\sin\theta_r,\\ k_c=\beta\dfrac{d_r}{2}\cos\theta_r\sin\theta_e\approx\beta\dfrac{d_r}{2}\cos(\theta_r)\theta_e.\end{cases} \tag{5}$$

Under conditions of cross-eye jamming, the sum- and difference-channel returns for the true target must be multiplied by the sum-channel antenna gain to ensure that they are equivalent to the jammer results. The total sum- and difference-channel returns for both the platform and the cross-eye jammer can thus be given as (du Plessis et al., 2009)

$$\begin{aligned}S_t=&S_j+a_se^{j\phi_s}S_g^2\\\approx&\frac{1}{2}[P_r(\theta_r)]^2[(1+ae^{j\phi}+a_se^{j\phi_s})(\cos(2k)+1)],\end{aligned} \tag{6}$$

$$\begin{aligned}D_t=&D_j+a_se^{j\phi_s}S_gD_g\\\approx&\mathrm{j}\frac{1}{2}[P_r(\theta_r)]^2[(1+ae^{j\phi}+a_se^{j\phi_s})\sin(2k)\\&+(1-ae^{j\phi})\sin(2k_c)],\end{aligned} \tag{7}$$

where the platform skin return will have an amplitude scaling of $a_s$ and a phase shift of $\phi_s$ relative to the return from one direction through the cross-eye jammer.

Under the assumptions in du Plessis (2012), the total monopulse ratio can be approximated as

$$\begin{aligned}M_t\approx&\frac{\sin(2k)}{\cos(2k)+1}\\&+\Re\left(\frac{1-ae^{j\phi}}{1+ae^{j\phi}+a_se^{j\phi_s}}\right)\frac{\sin(2k_c)}{\cos(2k)+1},\end{aligned} \tag{8}$$

where the cross-eye gain would be given by

$$G_{Ct}=\Re\left(\frac{1-ae^{j\phi}}{1+ae^{j\phi}+a_se^{j\phi_s}}\right). \tag{9}$$

Therefore, the ultimate monopulse ratio can be expressed as

$$M_t\approx\frac{\sin(2k)}{\cos(2k)+1}+G_{Ct}\frac{\sin(2k_c)}{\cos(2k)+1}, \tag{10}$$

where both the cross-eye jamming signal and platform skin return are within the received echoes, and the first term acts as a beacon while the second term causes an angular error. The error portion of this monopulse ratio consists of two factors, one of which depends on the jammer parameters and the radar cross section of the platform while the other depends on the geometry of the engagement. Obviously, the target signal and jamming signal compose the echoes in the monopulse radar. In the presence of monopulse radar, the echo model can be described as "multiple targets," which include the true target and the artificially apparent target induced by jamming.

### 2.2 Echo model with a random finite set

As above mentioned, to improve the target detection probability under the powerful jamming, a low threshold detection strategy was adopted, resulting in a rapid increase of the number of over-threshold detections. The measurement set obtained after a low-threshold constant false alarm rate (CFAR) was modeled as an RFS, in which target measurement, jamming measurement, and false alarm measurement are all included (Vo, 2008). The measurement set $Z=\{z_i\}_{i=1}^{M}$ that contains $M$ observations can be expressed as $Z=W\cup\tilde{W}\cup C$, where $W$ is the target observation, $\tilde{W}$ the jamming observation, and $C$ the false alarm observation. They are all expressed by the RFS as

$$W=\begin{cases}\varnothing, & \text{no target exists,}\\ \{w_1\}, & \text{one target exists,}\end{cases} \tag{11}$$

$$\tilde{W}=\begin{cases}\varnothing, & \text{no jamming exists,}\\ \{\tilde{w}_1\}, & \text{one jamming exists,}\end{cases} \tag{12}$$

$$C=\begin{cases}\varnothing, & \text{no false alarm exists,}\\ \{c_1\}, & \text{one false alarm exists,}\\ \{c_1,c_2\}, & \text{two false alarms exist,}\\ \quad\vdots & \quad\vdots\\ \{c_i\}_{i=1}^{n}, & n \text{ false alarms exist.}\end{cases} \tag{13}$$

Cross-eye jamming usually occurs after the target platform has been tracked and locked by a monopulse radar. It is possible to construct the measurement set in the following situations: (1) the measurement set includes only the observation of a false alarm, $Z=C$; (2) the measurement set includes the target and a false alarm, without jamming, $Z=W\cup C$; (3) the measurement set includes the target, a false alarm, and jamming at the same time, $Z=W\cup\tilde{W}\cup C$.

Typical multiple targets mixed with observations under cross-eye jamming are shown in Fig. 2, where the radar observations are mixed with target observations, jamming observations, and a large number of false alarm signals.

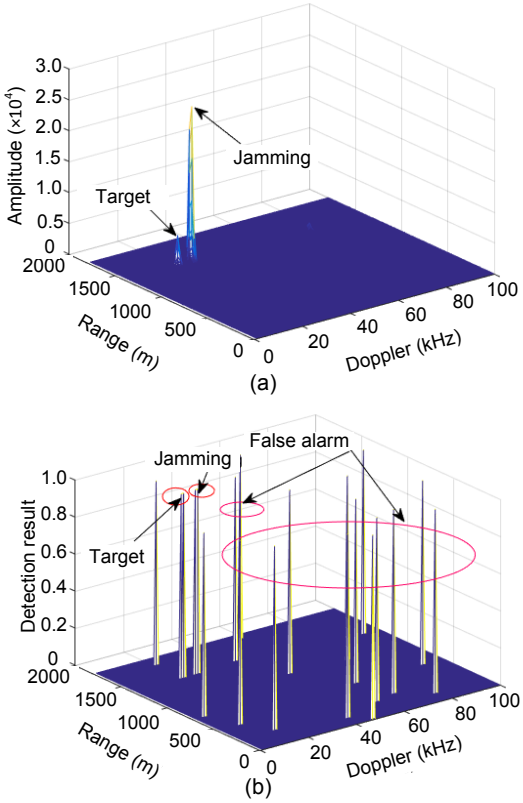


**Fig. 2 Target, jamming signals, and the corresponding radar observations: (a) signals in the range-Doppler (R-D) plane; (b) mixed radar observations**

## 3 Joint detection and tracking under a multi-target model

There are various situations that may occur within complex jamming environments, such as a newborn target, target derivation, target disappearances, jamming, and missed detection. Accurate information about the number of targets in the radar beam is difficult to obtain by monopulse radar at

every moment, which leads to many uncertainties. On the other hand, due to the lack of prior information about the tracking environment and uncertainty in target detection and tracking, the correlation between the target echo and the signal source becomes blurred. Monopulse radar cannot determine whether the source of the observation is from the actual target, clutter, or jamming. This will lead to the problem of combination explosion, and increase the computational complexity of the traditional multi-target tracking method based on data association. It becomes particularly difficult to deal with multi-target tracking situations, where the number of targets is unknown and changes over time.

Under the RFS framework, there are serval typical multi-target tracking filters, such as the PHD filter, cardinalized probability hypothesis density (CPHD) filter, multi-Bernoulli filter, and generalized labeled multi-Bernoulli (GLMB) filter. These filters are approximations of a multi-target Bayes filter based on different assumptions (Hong et al., 2011). The PHD filter is equivalent to the optimal multi-target Bayesian filter, when the assumption that both the multi-target state and the false alarm obey the Poisson group process is established (Ulmke et al., 2007). The computation and storage complexity of the PHD filter is much lower than that of the multi-target Bayesian filter, and the model has a wide range of applications with the outstanding ability for anti-false alarm and high estimation accuracy of the multi-target state (Vo et al., 2007). The time and measurement updates of the CPHD filter are based on the same modeling assumptions as the PHD filter, except that the clutter RFS is an independent and identically distributed cluster process (Vo et al., 2008). Unlike the PHD filter, the CPHD filter does not include a formal model for target spawning. The CPHD filter is essentially only a part of the second-order moments of a multi-target Bayesian filter (Vo et al., 2009). The assumption for distribution in the multi-Bernoulli filter is the multi-Bernoulli process, and the Bernoulli filter is just the multi-target Bayes filter, given that the number of targets is known a prior to be 0 or 1 (Vo et al., 2008; Vo and Vo, 2013). The GLMB filter is an exact closed-form multi-target filter, and is the first tractable provably Bayes-optimal multi-target detection and tracking algorithm (Papi et al., 2015; Beard et al., 2016). Under suitable approximations, the GLMB filter can be made efficient with regard to both tracking performance and computational throughput (Fantacci and Papi, 2016; Bryant et al., 2018).

The PHD, CPHD, multi-Bernoulli, and GLMB filters based on different assumptions have certain effect on multi-target tracking under complex environments, and each has its own advantages and disadvantages. Specific to multi-target detection and tracking applications under cross-eye jamming based on signal and model analysis conclusions, the measurements obtained by monopulse radar from the target and jamming can be modeled as a typical target-spawning process, and the generation of jamming observation has obvious correlation with the true target. Based on the target-spawning model characteristic of the PHD filter, the PHD filter with identity labels is a potential approach for realizing accurate detection, state estimation, and target recognition under angular deception jamming, from the aspects of model matching, algorithm performance, and computational complexity among the multi-target tracking filters.

### 3.1 Standard PHD for multi-target tracking

The PHD filter is a first-order statistical moment approximation of the full probability density function for multiple targets within the RFS framework. It solves the problem of the actual execution degree of RFS and avoids the difficulty to solve the full probability density (Shi et al., 2013). It is the optimal Poisson approximation of the posterior probability density for multi-target RFS under the Kullback-Leibler information criterion. The PHD filter helps avoid the recursion of the multi-target Bayesian filter in the RFS space, and greatly reduces computational complexity. The number of targets present in a radar beam can be estimated through the integration of the PHD, and the peak of the PHD corresponds to the estimated state of the targets. Thus, the PHD filter improves the tracking accuracy for multiple targets and at the same time ensures the real-time effectiveness of the resultant algorithm.

In the PHD filter, the first-order moment approximation of multi-target posterior density $D_{k|k}(x|Z^{(k)})$ is adopted to express the density function of the multi-target posterior density $p(x_k|Z^{(k)})$ at the $k^{\text{th}}$ moment. Thus, the prediction equation for the PHD filter is constructed as follows (Mahler, 2003):

$$D_{k|k-1}(x \mid Z^{(k-1)}) = \gamma_k(x) + \int \phi_{k|k-1}(x, x_{k-1}) D_{k-1|k-1}(x_{k-1} \mid Z^{(k-1)}) \mathrm{d}x_{k-1}, \tag{14}$$

where $\phi_{k|k-1}=b_{k|k-1}(x|\xi)+e_{k|k-1}(\xi)f_{k|k-1}(x|\xi)$, $b_{k|k-1}(\cdot|\xi)$ represents the spawned target set of the PHD, $B_{k|k-1}=(\{\xi\})$ of $e_{k|k-1}(\cdot)$ represents the probability of the existence of the target, $f_{k|k-1}(\cdot|\cdot)$ represents the transfer probability density of a single target, and $\gamma_k(\cdot)$ represents the newborn target set $\Gamma_k$ of the PHD.

The state update equation of the PHD filter is expressed as follows (Mahler, 2003):

$$D_{k|k}(x \mid Z^{(k)}) = L_{Z_k}(x) D_{k|k-1}(x \mid Z^{(k-1)}), \tag{15}$$

where

$$L_{Z_k}(x) = 1 - P_{D,k}(x) + \sum_{z \in Z_k} \frac{P_{D,k}(x) L_z(x)}{\lambda_k c_k(z) + D_{k|k-1}(P_{D,k} L_z)}. \tag{16}$$

$L_z(x)$ is the likelihood function for single target observation, $\lambda_k$ represents clutter intensity, $c_k(z)$ represents the spatial distribution of clutter, and $\lambda_k c_k(z)$ represents the clutter RFS of the PHD.

$$D_{k|k-1}(P_{D,k} L_z) = \int P_{D,k}(x) L_z(x) D_{k|k-1}(\boldsymbol{x} \mid Z^{(k-1)}) \mathrm{d}x, \tag{17}$$

where $P_{D,k}(\cdot)$ is the detection probability.

Although the PHD filter effectively avoids the data association problem, its output includes only the discrete number and state information of the target. The correlation between the state estimation and the target identity in each frame cannot be obtained; thus, stable tracking of the target cannot be achieved (Xiao et al., 2015). Nevertheless, it is very important for monopulse radar to be able to distinguish the identity of targets present in the radar beam and obtain a stable trajectory of the true target. Therefore, it is necessary to combine the characteristics of target and jamming with a standard PHD filter to realize the association between the state estimations and identity attributes, to achieve accurate detection, estimation, and recognition of the true target.

### 3.2 Joint detection and tracking integrated with identity labels

The implementation of cross-eye jamming has its own characteristics and laws, and jamming is released as an ECM approach for deceiving monopulse radar when the target has been tracked and locked. Before cross-eye jamming is released, the trajectory of the target is determined based on measurement, which includes only the target echo and noise, and the identity label of the target is contained in its state vector. After release jamming, the radar measurements composed of target, jamming, and false alarm clutter correspond to state estimations of multiple targets with different identity labels (Reuter et al., 2014). Section 2.1 reveals the angular characteristic difference and relationship between the true target and the artificial target generated by jamming. Therefore, it is feasible to use the characteristic differences of the target and jamming to optimize the partition of state particles, and deliver the identity labels using the relevance between the state estimation before and after the jamming release. The multi-target joint detection and tracking process integrated with identity labels is shown in Fig. 3.

The joint detection and tracking process for target and jamming integrated with cross-eye jamming characteristics based on the sequential Monte-Carlo method is as follows:

1. Step 0 ($k$=0) (initialization)

For $i$=1, 2, …, $N_0$, the initial particles are sampled as $\boldsymbol{x}_0^{(i)} \sim D_{0|0}$ (the prior PHD (Vo et al., 2005)). The particle weight is represented as $\omega_0^{(i)}$; therefore, the mass is $\omega_0^{(i)} = \hat{T}_0 / N$. Let the labels of the initial particles be the same, represented as $L_0^I = 0$. The particle partition at step 0 is $P_0^I$. Then, $k$=1.

2. Step 1 ($k \geq 1$) (prediction)

$\hat{N}_{k-1}$ denotes the estimated target number at step $k-1$, and the corresponding particle partition is represented as $\{P_{k-1,1}, P_{k-1,2}, \cdots, P_{k-1,\hat{N}_{k-1}}\}$, where all particles in one set are assigned the same labels (Vo and Vo, 2013).

For $i$=1, 2, …, $n_{k-1}$, assume that $n_{k-1}$ particles exist at step $n_{k-1}$. Sample $\tilde{\boldsymbol{x}}_k^{(i)}$ from a proposed density of $q_k(\cdot \mid x_{k-1}^{(i)}, Z_k)$. The predicted weight is expressed as

$$\tilde{\omega}_{k|k-1}^{(i)} = \frac{\phi_{k|k-1}(\tilde{x}_k^{(i)}, x_{k-1}^{(i)})}{q_k(\tilde{x}_k^{(i)}, x_{k-1}^{(i)}, Z_k)} \omega_{k-1}^{(i)}. \tag{18}$$

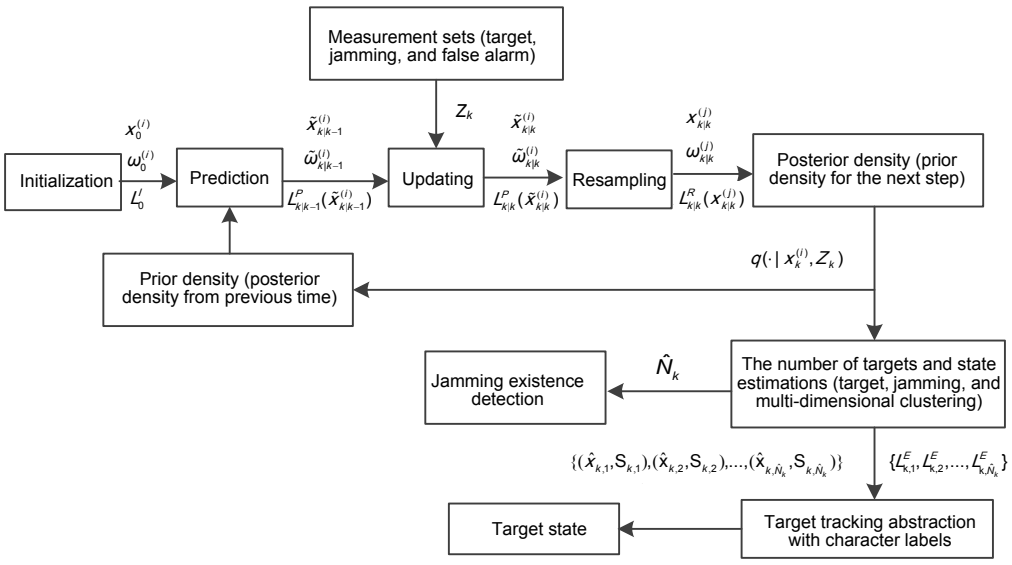


**Fig. 3 Flow process depicting the steps involved in joint detection and tracking of the multiple targets integrated with identity label**

Predicted labels for the particles are the same as those in the previous step:

$$L^{p}_{k|k-1}(x^{(i)}_{k|k-1}) = L^{p}_{k-1|k-1}(x^{(i)}_{k-1|k-1}). \tag{19}$$

For $i=n_{k-1}+1, n_{k-1}+2, \ldots, n_{k-1}+M$, where $M$ denotes the number of newborn particles, sample $\tilde{\boldsymbol{x}}^{(i)}_k$ from another proposed density of $p_k(\cdot \mid x^{(i)}_{k-1}, Z_k)$. The weight of newborn particles is expressed as

$$\tilde{\omega}^{(i)}_{k|k-1} = \frac{1}{M}\gamma_k(\tilde{x}^{(i)}_k) \big/ p_k(\tilde{x}^{(i)}_k \mid Z_k). \tag{20}$$

Labels of the newborn particles are given as

$$L^{p}_{k|k-1}(\boldsymbol{x}^{(i)}_{k|k-1}) = L_{k,\,\mathrm{new}}. \tag{21}$$

The prediction particle partition at step $k$ is expressed as

$$\begin{aligned}&\{P^{p}_{k,\,1},\ P^{p}_{k,\,2},\ \cdots,\ P^{p}_{k-1,\hat{N}_{k-1}+1}\}\\ &=\{P_{k-1,\,1},\ P_{k-1,\,2},\ \cdots,\ P_{k-1,\hat{N}_{k-1}}\}\cup P^{p}_{k,\,L_{k,\,\mathrm{new}}}.\end{aligned} \tag{22}$$

3. Step 2 ($k\geq 1$) (update)

When $z\in Z_k$, compute

$$<\tilde{\omega}_{k|k-1},\ \varphi_{k,\,z}>=\sum_{i=1}^{R_k}\varphi_{k,\,z}(\tilde{\boldsymbol{x}}^{(i)}_k)\tilde{\omega}^{(i)}_{k|k-1}, \tag{23}$$

where $R_k=N_{k-1}+M$ represents the total number of particles.

For $i=1, 2, \ldots, R_k$, the update weight is given as

$$\tilde{\omega}^{(i)}_k = \left(\nu(\tilde{\boldsymbol{x}}^{(i)}_k)+\sum_{z\in Z_k}\frac{\varphi_{k,z}(\tilde{\boldsymbol{x}}^{(i)}_k)}{\kappa_k(z)+<\tilde{\omega}_{k|k-1},\varphi_{k,z}>}\right)\tilde{\omega}^{(i)}_{k|k-1}. \tag{24}$$

The update state is kept constant, given as

$$\tilde{\boldsymbol{x}}^{(i)}_{k|k} = \boldsymbol{x}^{(i)}_{k|k-1}. \tag{25}$$

The update label is kept constant, given as

$$L^{U}_{k|k}(\tilde{\boldsymbol{x}}^{(i)}_{k|k}) = L^{p}_{k|k-1}(\boldsymbol{x}^{(i)}_{k|k-1}). \tag{26}$$

The prediction particle partition at step $k$ is given as

$$\{P^{U}_{k,1}, P^{U}_{k,2}, \cdots, P^{U}_{k-1,\hat{N}_{k-1}+1}\} = \{P^{p}_{k,1}, P^{p}_{k,2}, \cdots, P^{p}_{k-1,\hat{N}_{k-1}+1}\}. \tag{27}$$

4. Step 3 ($k\geq 1$) (resampling)

The total particle mass is computed as

$$\hat{N}_k = \sum_{i=1}^{R_k}\tilde{\omega}^{(i)}_k. \tag{28}$$

Set $J_k = p\hat{N}_k$, where $p$ denotes the number of particles for the single target. When $i=1, 2, \ldots, R_k, j=1,$

2, …, $J_k$, resampling yields the following results: the resample state is given as $\tilde{\boldsymbol{x}}_{k|k}^{(j)} = \text{child}(\tilde{\boldsymbol{x}}_{k|k}^{(i)})$, each resample particle has a weight of $\hat{N}_k / p$, and the resample label is given as $L_{k|k}^R(\boldsymbol{x}_{k|k}^{(j)}) = L_{k|k}^U(\tilde{\boldsymbol{x}}_{k|k}^{(i)})$. Particle partition after resampling is given as $\{P_{k,1}^R, P_{k,2}^R, \cdots, P_{k,\hat{N}_{k-1}+1}^R\}$.

5. Step 4 ($k$≥1) (estimation extraction)

There are some good extraction methods with high estimation accuracy and fast calculation speed, such as multi-expected a posteriori (MEAP) (Li et al., 2016, 2017). To retain and deliver the identity labels of states, the traditional clustering and re-clustering steps are introduced to obtain particle partitions.

For the number of estimated targets $\hat{N}_k$ and particle set $\{\boldsymbol{x}_k^1, \boldsymbol{x}_k^2, \cdots, \boldsymbol{x}_k^{(J_k)}\}$ obtained in step 3, all particles are clustered on the angle dimension, because cross-eye jamming will form a spurious angle, which is different from the true angle of the target (Clark and Bell, 2007).

(1) Step 4.1 (initialization center)

Set $h$:=1.

Randomly choose $\hat{N}_k$ particles from the particle set $\{\boldsymbol{x}_k^1, \boldsymbol{x}_k^2, \cdots, \boldsymbol{x}_k^{(J_k)}\}$ to be the initial center as the following:

$$\{\boldsymbol{m}_{k,1}^{(h)}, \boldsymbol{m}_{k,2}^{(h)}, \cdots, \boldsymbol{m}_{k,\hat{N}_k}^{(h)}\} \in \{\boldsymbol{x}_k^1, \boldsymbol{x}_k^2, \cdots, \boldsymbol{x}_k^{(J_k)}\}. \quad (29)$$

Establish $\hat{N}_k$ particle partitions $\{P_{k,1}^{(h)}, P_{k,2}^{(h)}, ..., P_{k,\hat{N}_k}^{(h)}\}$ to satisfy $\boldsymbol{m}_{k,n}^{(h)} \in P_{k,n}^{(h)}$, where $n$=1: $\hat{N}_k$.

(2) Step 4.2 (particle partition)

For $\boldsymbol{x}_k^{(i)}$, $i$=1:$J_k$:

Calculate $\| \boldsymbol{x}_k^{(i)} - \boldsymbol{m}_{k,n}^{(h)} \|$, and set $a$= $\arg\min_n \| \boldsymbol{x}_k^{(i)} - \boldsymbol{m}_{k,n}^{(h)} \|$. Then, $\boldsymbol{x}_k^{(i)} \in P_{k,a}^{(h)}$.

Sequentially calculate every particle and assign them to the corresponding partitions.

Set $h$=$h$+1.

(3) Step 4.3 (center recalculation)

Calculate the means of partitions as

$$\boldsymbol{m}_{k,n}^{(h)} = \text{mean}\,(P_{k,n}^{(h-1)}). \quad (30)$$

Calculate the formula as follows:

$$\left| \sum_{i=1}^{J_k} \sum_{n=1}^{\hat{N}_k} \| \boldsymbol{x}_k^{(i)} - \boldsymbol{m}_{k,n}^{(h)} \| - \sum_{i=1}^{J_k} \sum_{n=1}^{\hat{N}_k} \| \boldsymbol{x}_k^{(i)} - \boldsymbol{m}_{k,n}^{(h-1)} \| \right| < \varepsilon. \quad (31)$$

If inequality (31) holds, go to step 4.4; otherwise, repeat step 4.2 until inequality (31) holds.

(4) Step 4.4 (means and covariance calculation)

Compute the means of the partitions as

$$\hat{\boldsymbol{x}}_k^{(n)} = \text{mean}(P_{k,n}^{(h)}). \quad (32)$$

Compute the covariance of the partitions as

$$\hat{\boldsymbol{S}}_k^n = \text{cov}(P_{k,n}^{(h)}). \quad (33)$$

Output the means and covariance of the $\hat{N}_k$ partitions as $\{(\hat{\boldsymbol{x}}_k^{(1)}, \hat{\boldsymbol{S}}_k^{(1)}), (\hat{\boldsymbol{x}}_k^{(2)}, \hat{\boldsymbol{S}}_k^{(2)}), \cdots, (\hat{\boldsymbol{x}}_k^{\hat{N}_k}, \hat{\boldsymbol{S}}_k^{\hat{N}_k})\}$.

(5) Step 4.5 (re-clustering the particles)

Compute the relationship between $\hat{N}_k$ partitions, if any two state estimations $\hat{\boldsymbol{x}}_k^{(i)}$ and $\hat{\boldsymbol{x}}_k^{(j)}$ among $\{\hat{\boldsymbol{x}}_k^{(1)}, \hat{\boldsymbol{x}}_k^{(2)}, \cdots, \hat{\boldsymbol{x}}_k^{\hat{N}_k}\}$ satisfy

$$\exp\left\{ -\frac{1}{2} (\boldsymbol{H}\hat{\boldsymbol{x}}_k^{(i)} - \boldsymbol{H}\hat{\boldsymbol{x}}_k^{(j)})^{\mathrm{T}} \cdot (\boldsymbol{H}^{\mathrm{T}} \boldsymbol{S}_k^{(i)} \boldsymbol{H})(\boldsymbol{H}\hat{\boldsymbol{x}}_k^{(i)} - \boldsymbol{H}\hat{\boldsymbol{x}}_k^{(j)}) \right\} < \delta_\varepsilon, \quad (34)$$

where $\boldsymbol{H}$ represents the matrix of extraction of the position vector from the state vector, and $\delta_\varepsilon$ is a threshold used to measure the close relationship between two vectors. This indicates that there is a close relationship between the two state estimations, and the clustering is unreasonable.

Re-cluster the particle sets corresponding to $\hat{\boldsymbol{x}}_k^{(i)}$ and $\hat{\boldsymbol{x}}_k^{(j)}$ on the range dimension or/and velocity dimension, and form two new particle sets.

After re-clustering the particles, the final particle partition posterior state estimation is $\{P_{k,1}^E, P_{k,2}^E, \cdots, P_{k,\hat{N}_k}^E\}$. Different labels should be included in each individual partition, and the partition labels should be fixed in step 5.

6. Step 5 ($k$≥1) (sociation and track determination)

The final partition label is determined based on association and track extraction. The relationship between $\boldsymbol{x}_{k,i}$ and child($\tilde{\boldsymbol{x}}_{k,i}$) is compared with $P_{k,j}^{E}$ and $P_{k,j}^{R}$, following which two 0-1 MU and MR matrices are constructed as follows (Xiao et al., 2015):

$$\mathrm{MU}_{j,k}=\begin{cases}1, & \text{if } \left|\left\{i \mid \boldsymbol{x}_{k}^{(i)} \in P_{k,j}^{R} \cap P_{k,l}^{E}\right\}\right|>\varepsilon_1 J_k,\\ 0, & \text{otherwise,}\end{cases} \tag{35}$$

$$\mathrm{MR}_{j,k}=\left|\left\{i \mid \mathrm{child}(\tilde{\boldsymbol{x}}_{k}^{(i)}) \in P_{k,j}^{R} \cap P_{k,l}^{E}\right\}\right|, \tag{36}$$

where $j=1, 2, \cdots, \hat{N}_{k-1}+1$, $l=1, 2, \cdots, \hat{N}_k$, and $\varepsilon_1=1/(4\hat{N}_k)$.

For each $j=1, 2, \cdots, \hat{N}_{k-1}+1$, if $\sum_l \mathrm{MU}_{j,l}=0$, the target is dead and the target track that possesses the label for partition $P_{k,j}^{R}$ is also deleted. If $\sum_l \mathrm{MU}_{j,l}=1$, for particle partition $P_{k,p}^{E}$ satisfying $\mathrm{MU}_{j,p}=1$ when $P_{k,p}^{E}$ is unlabeled, the label of partition $P_{k,p}^{R}$ is set as its label and target survival is declared. When the label of $P_{k,p}^{E}$ is not included in the corresponding label set, the steps are continued. When the label of $P_{k,p}^{E}$ is included in the label set and $\mathrm{MU}_{j,p}>\mathrm{MU}_{j',p}$, partition $P_{k,j}^{R}$ is set as the label of $P_{k,p}^{E}$; otherwise, the steps are continued until such conditions are reached.

If $\sum_l \mathrm{MU}_{j,l}>1$, when $P_{k,p}^{E}$ satisfies $p=\max_l \mathrm{MR}_{j,l}$ and $\mathrm{MU}_{j,p}=1$, the label of partition $P_{k,j}^{R}$ is set as its label and the target survival is declared.

When $P_{k,p}^{E}$ satisfies $\mathrm{MU}_{j,q}=1$ ($q\neq p$), a new label is assigned to the existing labels, and the target spawn is declared.

If there still exists an unlabeled partition, a new label is assigned to the existing labels, and the target birth is declared.

By running a filter, the number of estimated targets can be used to determine the presence of jamming, and the monopulse radar can successfully distinguish the target and jamming based on the different identity labels.

## 4 Simulation verification of the algorithm

### 4.1 Measurement and state model

Experiments were performed wherein the relative motion and dynamic geometry of monopulse radar and the target under cross-eye jamming were simulated. To simplify the analysis, it was assumed that the radar was always at the coordinate origin, and the target was modeled using a nearly constant turn (NCT) model (Li and Jilkov, 2003). The target flew towards the radar, and the two jammers for cross-eye jamming were onboard on the wing of the plane in Fig. 4. The parameters and setting of the scene are shown in Table 1.

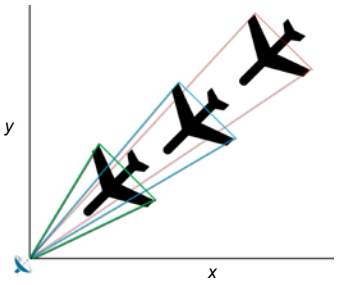


**Fig. 4 A sketch depicting the target and jamming mapped in a two-dimensional (2D) plane**

Here, the target state is denoted by $\boldsymbol{x}_k=[x_k, \dot{x}_k, y_k, \dot{y}_k]^{\mathrm{T}}$, where $(x_k, y_k)$ is the center of the target and $(\dot{x}_k, \dot{y}_k)$ is the velocity of the target. The state transition equation is as follows:

$$\boldsymbol{x}_k=\boldsymbol{F}\boldsymbol{x}_{k-1}+\boldsymbol{G}\boldsymbol{w}_{k-1}, \tag{37}$$

where

$$\boldsymbol{F}=\begin{bmatrix}1 & T & 0 & 0\\ 0 & 1 & 0 & 0\\ 0 & 0 & 1 & T\\ 0 & 0 & 0 & 1\end{bmatrix}, \tag{38}$$

$$\boldsymbol{G}=\begin{bmatrix}T^2/2 & T & 0 & 0\\ 0 & 0 & T^2/2 & T\end{bmatrix}^{\mathrm{T}}. \tag{39}$$

$\boldsymbol{w}_{k-1}=[w_{x,k-1}, w_{y,k-1}]^{\mathrm{T}}$ is a vector for processing noise, which is zero-mean Gaussian with standard deviations of $\sigma_x=\sigma_y=100$ m/s$^2$, and $T$ is the sampling period.

**Table 1 Parameters used in the simulation**

| Parameter type | Parameter | Value |
|---|---|---|
| Target parameters | Initial range $R$ | 5 km |
| | Initial velocity $V$ | 1200 m/s |
| | Fly direction | Toward a target |
| | Amplitude scaling $a_s$ | 0.02 |
| | Phase shift $\phi_s$ | 30° |
| Jamming parameters | Time of releasing | The 11th step |
| | Baseline length | 20 m |
| | Amplitude ratio $a$ | 0.95 |
| | Phase difference $\phi$ | 175° |
| | Range difference relative to the target | 10 m |
| | Velocity difference relative to the target | 6 m/s |
| Radar parameters | Beam width | 5° |
| | Line of sight direction | Toward a target |
| Other parameters | Measuring period | 6 ms |
| | Initial signal-to-noise ratio | 0 dB |
| | Equivalent jamming-to-signal ratio | 34 dB |
| | Total simulation time | 1 s |

The radar observations include range, velocity, and azimuth for the target, and the observation equation for the target is expressed as follows:

$$\boldsymbol{z}_k=\left[\sqrt{x_k^2+y_k^2},\ \frac{x_k\dot{x}_k}{\sqrt{x_k^2+y_k^2}}+\frac{y_k\dot{y}_k}{\sqrt{x_k^2+y_k^2}},\ \arctan\left(\frac{y_k}{x_k}\right)\right]^{\mathrm{T}}+[\boldsymbol{w}_{r,k},\ \boldsymbol{w}_{p,k},\ \boldsymbol{w}_{\theta,k}]^{\mathrm{T}}, \tag{40}$$

where $\boldsymbol{w}_{r,k}$, $\boldsymbol{w}_{p,k}$, and $\boldsymbol{w}_{\theta,k}$ are zero-mean Gaussian noise vectors in the range and azimuth, with standard deviations of $\sigma_{w_{r,k}}$=5 m, $\sigma_{w_{p,k}}$=3 m/s, and $\sigma_{w_{\theta,k}}$=0.3 mrad/s, respectively. The simulation involved 250 time cycles. The true scene for the simulation is shown in Fig. 5.

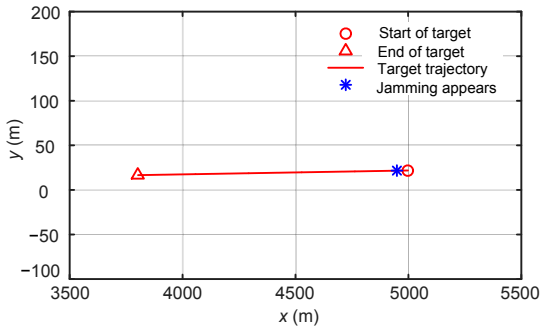


**Fig. 5 True scene for the simulation**

In Fig. 5, the start and end of target motions are marked and the target trajectory is traced between them. Cross-eye jamming is released during the 11th step cycle, and the jamming is shown. According to the cross-eye jamming course, the jamming is released by the target after the target has been detected and tracked stably by monopulse radar, and the low threshold of CFAR detection is introduced; thus, the detection probability of the target is assumed to be $p_D$=1, and the survival probability of the target is set to $p_S$=0.99.

The mixed measurements obtained by monopulse radar are shown in Fig. 6. It can be seen that many measurements are obtained at every moment, including observations of the target, jamming, and false alarm signals. Due to the low threshold detection, there are many points exceeding the detection threshold at each moment. Therefore, monopulse radar needs to detect, track, and distinguish the target in the observations with high false alarms.

In the simulation, to fully verify the performance of the proposed algorithm in terms of the detection and estimation accuracy under the influence of powerful jamming, multiple Monte-Carlo experiments were conducted. The number of Monte-Carlo experiments was 100, with the simulation scenario and parameters described in Fig. 3 and Table 1, respectively. The initial parameters of the joint detection and tracking were set as follows: the number of

particles for simulating a single target was 2000, and the number of newborn particles was 200. Successive sampling was based on the last observation.

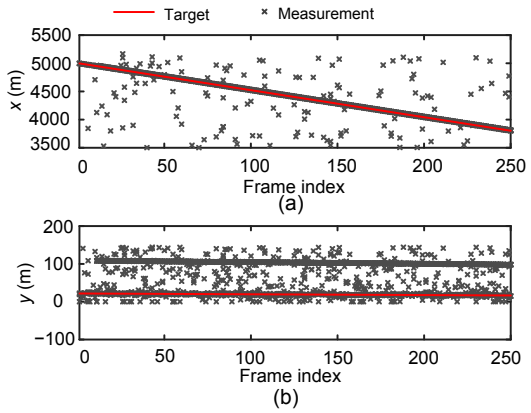


**Fig. 6 Mixed measurements for the monopulse radar after CFAR detection in the *x* (a) and *y* (b) axes**

## 4.2 Simulation results

The detection accuracy and delay for jamming release are the main indicators to examine the performance of the algorithm. The proposed algorithm detects and decides jamming release based on the number of estimated stable targets. During the processing, if the number of estimated targets is one, it indicates the presence of a true target in the scenario alone; if the number of the estimated targets is two, it indicates the appearance of jamming, and both the true target and the jamming are within the radar beam.

Fig. 7 depicts the average statistical results for the estimation number, and it can be seen that the proposed algorithm is accurate in estimating the number of targets present within the radar beam. When cross-eye jamming is released, the change in echo can be quickly detected by the algorithm and reflected in changes in the number of the estimated targets. In Fig. 7, it can be seen that the delay for detecting jamming is small. The cross-eye jamming is released during the $11^{th}$ step, and the monopulse radar detects the number of changed targets in the $12^{th}$ step in most cases. The average detection delay is only one frame period, which means that real-time detection of jamming is highly effective.

State estimation accuracy and target recognition accuracy are other indicators of the algorithm performance. That is to say, the proposed algorithm must not only estimate the target state, but also discriminate the target and jamming, thus obtaining stable tracking to the true target. The ultimate goal is to make the monopulse radar stably track the true target, rather than track the jamming or the energy centroid of both.

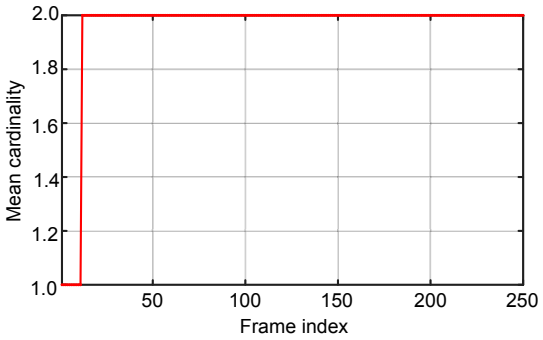


**Fig. 7 Average of the estimation results for the number of targets at each moment**

The state estimation performed by the traditional PHD filter without combining the identity labels is shown in Fig. 8. It can be seen that the traditional PHD filter can obtain the states of all targets in the radar beam according to the observations. However, since the target identity information is not added in the filtering process, the association between the target state and target identity is not obtained. Therefore, the filtering results are some isolated state values, there is no stable track corresponding to the target attribute, and it is not clear whether the state is the target or jamming.

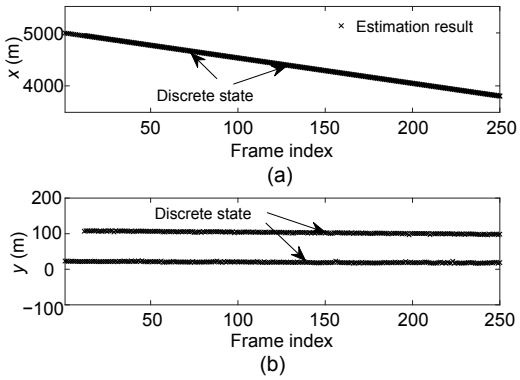


**Fig. 8 State estimation for the traditional PHD filter in the *x* (a) and *y* (b) axes**

The proposed algorithm adds identity information in the filtering process through labels based on the traditional PHD filter. Therefore, it is possible to effectively correlate the estimated state with the target

attribute, not only to obtain continuous tracking, but also to discriminate the target and jamming based on identity labels. Fig. 9 shows the results of the proposed algorithm. It can be seen that, compared with the results of the traditional PHD filter in Fig. 8, after adopting the label PHD, continuous tracking of the true target state can be released by associating the estimated state with the identity label. It marks the distinction between the target and jamming, and finally outputs only the stable track of the target.

To further illustrate the performance of the proposed algorithm under cross-eye jamming, the true target value and the estimated state value obtained based on labels are compared in a two-dimensional (2D) plane. In Fig. 10, it can be seen that, the state estimation for the target obtained by the proposed algorithm is always close to the true target location under cross-eye jamming.

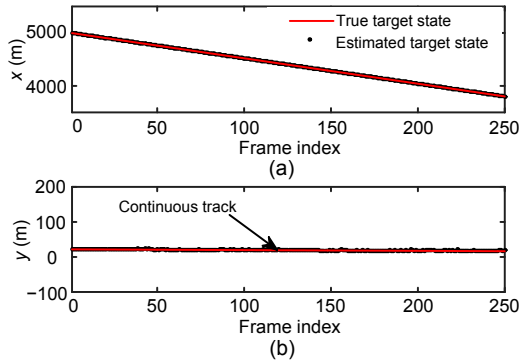


**Fig. 9 State estimation obtained using the proposed algorithm in the *x* (a) and *y* (b) axes**

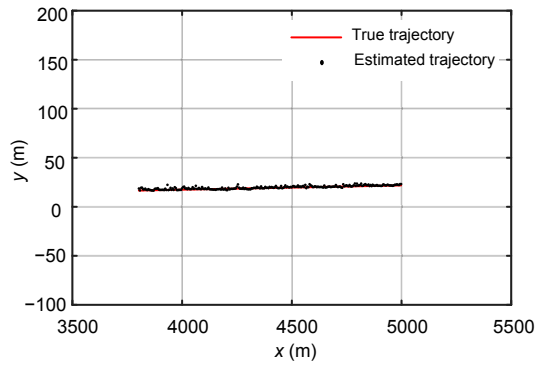


**Fig. 10 Two-dimensional estimated state results for the proposed algorithm**

The accuracy of the estimated state value for the target is determined by comparing the degree of the deviation between the estimation result and the true value. Specific indicators include the optimal sub-pattern assignment (OSPA) distance, the estimation errors in the *x* and *y* axes, and the range and angle estimation errors (Schuhmacher et al., 2008). The average performance of the state estimation for 100 experiments is shown in Figs. 11–13.

The average OSPA error curve for the 100 Monte-Carlo experiments is shown in Fig. 11. It can be seen that the average OSPA error for the target with the proposed algorithm is less than 3 m. It indicates that the proposed algorithm has a high estimation accuracy, and the estimated value is close to the true value throughout the filtering process. In the whole anti-jamming process, the proposed algorithm can effectively distinguish the target and the jamming, thus ensuring that the true target can be tracked stably and reliably all the time, without error tracking in the jamming or loss of the target.

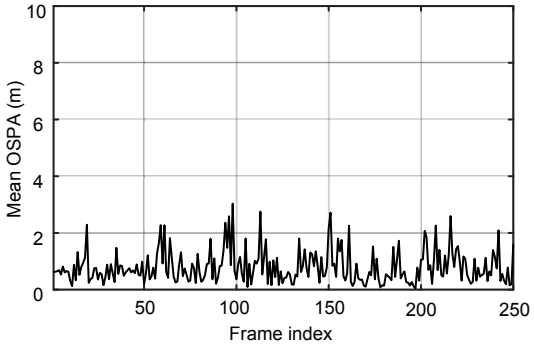


**Fig. 11 OSPA error performance for target tracking**

Figs. 12 and 13 show the estimation error curves for tracking the true target in the *x* and *y* axes, together with range and angle estimation errors. It can be seen that the estimation errors in the *x* and *y* axes are both less than 3 m in the Cartesian coordinate system. In the polar coordinate system, the angle estimation errors are very small, thus ensuring that the monopulse radar always points to the true target without being disturbed. As noted earlier, the essence of cross-eye jamming is to generate a large angle error in monopulse angle measurement and cause the radar to point to an artificial target located some distance away from the true target. The proposed algorithm enables the correct estimation of the range and angle of the true target to avoid being tricked, and these results verify its effectiveness in counteracting cross-eye jamming.

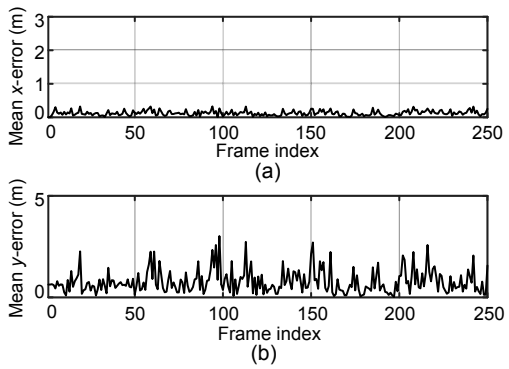


**Fig. 12 Target estimation errors in the $x$ (a) and $y$ (b) axes**

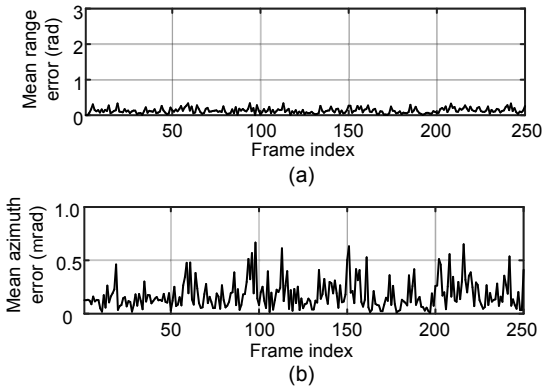


**Fig. 13 Range (a) and angle (b) estimation errors**

## 5 Conclusions

In this study, we have proposed and investigated an algorithm for counteracting typical cross-eye jamming for monopulse radar. Through detailed analysis of the jamming principle and establishment of a random set multi-target model, a novel anti-jamming method based on the PHD filter has been developed combining the characteristic differences between the target and jamming with the jamming release processing information. The simulation results showed that the proposed algorithm can detect the release of jamming with high probability and small delay, and can achieve an accurate state estimation and correct target recognition. The tracking error for the true target has been found to be small, ensuring that the monopulse radar retains the correct bearing and table track for the true target.

### Compliance with ethics guidelines

Zhi-yong SONG, Xing-lin SHEN, and Qiang FU declare that they have no conflict of interest.

## References

Bai K, Wang YH, 2013. Millimeter-wave radar and IR fusion anti-jamming method based on the analysis of target activities. *J Huazhong Univ Sci Technol* (*Nat Sci Ed*), 41(S1):163-166 (in Chinese). https://doi.org/10.13245/j.hust.2013.s1.047

Beard M, Reuter S, Granström K, et al., 2016. Multiple extended target tracking with labeled random finite sets. *IEEE Trans Signal Process*, 64(7):1638-1653. https://doi.org/10.1109/TSP.2015.2505683

Bryant DS, Vo BT, Vo BN, et al., 2018. A generalized labeled multi-Bernoulli filter with object spawning. *IEEE Trans Signal Process*, 66(23):6177-6189. https://doi.org/10.1109/TSP.2018.2872856

Clark DE, Bell J, 2007. Multi-target state estimation and track continuity for the particle PHD filter. *IEEE Trans Aerosp Electron Syst*, 43(4):1441-1453. https://doi.org/10.1109/TAES.2007.4441750

du Plessis WP, 2012. Platform skin return and retrodirective cross-eye jamming. *IEEE Trans Aerosp Electron Syst*, 48(1):490-501. https://doi.org/10.1109/TAES.2012.6129650

du Plessis WP, 2016. Path-length effects in multiloop retrodirective cross-eye jamming. *IEEE Antenn Wirel Propag Lett*, 15:626-629. https://doi.org/10.1109/LAWP.2015.2465815

du Plessis WP, Odendaal JW, Joubert J, 2009. Extended analysis of retrodirective cross-eye jamming. *IEEE Trans Antenn Propag*, 57(9):2803-2806. https://doi.org/10.1109/TAP.2009.2027353

du Plessis WP, Odendaal JW, Joubert J, 2011. Experimental simulation of retrodirective cross-eye jamming. *IEEE Trans Aerosp Electron Syst*, 47(1):734-740. https://doi.org/10.1109/TAES.2011.5705704

Fantacci C, Papi F, 2016. Scalable multisensor multitarget tracking using the marginalized δ-GLMB density. *IEEE Signal Process Lett*, 23(6):863-867. https://doi.org/10.1109/LSP.2016.2557078

Hong S, Wang L, Shi ZG, et al., 2011. Simplified particle PHD filter for multiple-target tracking: algorithm and architecture. *Prog Electromagn Res*, 120:481-498. https://doi.org/10.2528/PIER11081901

KRET, 2014. Missiles are not a problem: the SAP 518 jamming station protects fighter jets from guided missiles. http://www.kret.com/en/news/3544/

Li J, Shen W, 2015. Analysis of anti-jamming capability of multistatic radar system under different interference rules. *Acta Armam*, 36(S2):178-185 (in Chinese).

Li TC, Sun SD, Corchado JM, et al., 2014. A particle dyeing approach for track continuity for the SMC-PHD filter. Proc 17th IEEE Int Conf on Information Fusion, p.1-8.

Li TC, Corchado JM, García J, et al., 2016. MEAP: approximate optimal estimate extraction for the SMC-PHD filter. Proc 19th IEEE Int Conf on Information Fusion, p.2309-2316.

Li TC, Corchado JM, Sun SD, et al., 2017. Multi-EAP:

extended EAP for multi-estimate extraction for SMC-PHD filter. *Chin J Aeronaut*, 30(1):368-379. https://doi.org/10.1016/j.cja.2016.12.025

Li XR, Jilkov VP, 2003. Survey of maneuvering target tracking. Part I. Dynamic models. *IEEE Trans Aerosp Electron Syst*, 39(4):1333-1364. https://doi.org/10.1109/TAES.2003.1261132

Li YZ, Hu WQ, Chen X, et al., 2013. Research on polarization discrimination algorithm for coherent dual-source angle deception interference. *Acta Armam*, 34(9):1078-1083 (in Chinese). https://doi.org/10.3969/j.issn.1000-1093.2013.09.004

Lin L, Bar-Shalom Y, Kirubarajan T, 2006. Track labeling and PHD filter for multitarget tracking. *IEEE Trans Aerosp Electron Syst*, 42(3):778-795. https://doi.org/10.1109/TAES.2006.248213

Mahler RPS, 2003. Multitarget Bayes filtering via first-order multitarget moments. *IEEE Trans Aerosp Electron Syst*, 39(4):1152-1178. https://doi.org/10.1109/TAES.2003.1261119

Mahler RPS, 2007. Statistical Multisource Multitarget Information Fusion. Artech House, Norwood, MA, USA, p.194-211.

Mahler RPS, 2014. Advances in Statistical Multisource-Multitarget Information Fusion. Artech House, Norwood, MA, USA, p.307-329.

Papi F, Vo BN, Vo BT, et al., 2015. Generalized labeled multi-Bernoulli approximation of multi-object densities. *IEEE Trans Signal Process*, 63(20):5487-5497. https://doi.org/10.1109/TSP.2015.2454478

Reuter S, Vo BT, Vo BN, et al., 2014. The labeled multi-Bernoulli filter. *IEEE Trans Signal Process*, 62(12):3246-3260. https://doi.org/10.1109/tsp.2014.2323064

Schuhmacher D, Vo BT, Vo BN, 2008. A consistent metric for performance evaluation of multi-object filters. *IEEE Trans Signal Process*, 56(8):3447-3457. https://doi.org/10.1109/TSP.2008.920469

Shi ZG, Zheng Y, Bian X, et al., 2013. Threshold-based resampling for high-speed particle PHD filter. *Prog Electromagn Res*, 136:369-383. https://doi.org/10.2528/PIER12120406

Ulmke M, Erdinc O, Willett P, 2007. Gaussian mixture cardinalized PHD filter for ground moving target tracking. Proc 10th Int Conf on Information Fusion, p.1-8. https://doi.org/10.1109/ICIF.2007.4408105

Vo BN, Sing S, Doucet A, 2005. Sequential Monte Carlo methods for multi-target filtering with random finite sets. *IEEE Trans Aerosp Electron Syst*, 41(4):1224-1245. https://doi.org/10.1109/TAES.2005.1561884

Vo BT, 2008. Random Finite Sets in Multi-object Filtering. PhD Thesis, University of Western Australia, Australia, p.127-144.

Vo BT, Vo BN, 2013. Labeled random finite sets and multi-object conjugate priors. *IEEE Trans Signal Process*, 61(13):3460-3475. https://doi.org/10.1109/TSP.2013.2259822

Vo BT, Vo BN, Cantoni A, 2007. Analytic implementations of the cardinalized probability hypothesis density filter. *IEEE Trans Signal Process*, 55(7):3553-3567. https://doi.org/10.1109/TSP.2007.894241

Vo BT, Vo BN, Cantoni A, 2008. Bayesian filtering with random finite set observations. *IEEE Trans Signal Process*, 56(4):1313-1326. https://doi.org/10.1109/TSP.2007.908968

Vo BT, Vo BN, Cantoni A, 2009. The cardinality balanced multi-target multi-Bernoulli filter and its implementations. *IEEE Trans Signal Process*, 57(2):409-423. https://doi.org/10.1109/TSP.2008.2007924

Wu W, Wang GH, Liu Y, et al., 2011. Airborne radar/IRST/ESM synergistic tracking and management. *Syst Eng Electron*, 33(7):1517-1522 (in Chinese). https://doi.org/10.3969/j.issn.1001-506X.2011.07.16

Xiao HT, Li YX, Fu Q, 2015. Identification and tracking of towed decoy and aircraft using multiple-model improved labeled P-PHD filter. *Dig Signal Process*, 46:49-58. https://doi.org/10.1016/j.dsp.2015.07.005

Xue D, Dong WF, Gao JM, et al., 2011. Performance analysis of time-domain discrimination technique of ARUAV on countering three active sources. *Radar Sci Technol*, 9(6):496-501. https://doi.org/10.3969/j.issn.1672-2337.2011.06.003

Zhao SS, Zhang LR, Zhou Y, et al., 2014. Measurement fusion method against false-target jamming for radar network. *J Univ Electron Sci Technol China*, 43(2):207-211. https://doi.org/10.3969/j.issn.1001-0548.2014.02.009